United States Air Force Investigation and Evaluation of Composite Scarf Repairs

David Mollenhauer & Kara Storage
U.S. Air Force Research Laboratory
2941 Hobson Way
Wright Patterson AFB, Ohio 45433-7750
UNITED STATES OF AMERICA
david.mollenhauer@us.af.mil & kara.storage@us.af.mil

Michael Czabaj, Jason Hamburg, Dallan Barnes, & Nicolas Dorsett
The University of Utah
1471 E. Federal Way
Salt Lake City, Utah 84112
UNITED STATES OF AMERICA

Daniel Rapking
The University of Dayton Research Institute
300 College Park
Dayton, OH 45469
UNITED STATES OF AMERICA

ABSTRACT

With increasing numbers of composite aircraft entering service in the United States Air Force (USAF), damage repair strategies are of great importance. Repair methods used in composite structures can differ significantly from those used for metallic structures. Oftentimes, a bonded "scarf" repair is used on composite structures in which the damaged area is removed at a tapered angle, or "scarfed out," and then the area is filled with layers of adhesive and composite material to restore the repair area. Scarf repairs can be efficient in restoring load-carrying capacity to a damaged composite laminate, but certification challenges exist limiting full structural credit to be given for these repairs. One of the reasons limiting confidence in the structural repair is the USAF currently lacks experimental methods and numerical tools to understand the progressive nature of damage and failure of scarf repairs, analyze and optimally design scarf repairs, and predict in-service performance of these scarf repairs. In this effort, the Air Force Research Laboratory's (AFRL) in-house progressive damage tool, BSAM, is assessed for prediction of damage and failure of scarf repairs. To date, BSAM has been used for the simulation of damage in a variety of idealized composite geometries and damage states. This effort aims to extend the use of BSAM beyond its research realm by applying it to practical engineering repairs related to the USAF sustainment mission. The following tasks will be completed: material characterization of the parent composite material, two-dimensional (2D) calibration experiments of scarf joints, BSAM numerical simulations to establish its predictive capability, and ultimately 2D and three-dimensional (3D) uniaxial and biaxial testing of representative composite scarf repairs. The major project outcomes include extending the use of BSAM to practical engineering problems related to the USAF sustainment mission, identifying possible upgrades/modifications to BSAM to broaden its user base, and formulating a framework/methodology for streamlined deployment of BSAM for existing and future composite aircraft structures within the USAF.

1.0 PROGRAM OVERVIEW

With increasing numbers of composite-intensive aircraft entering service in the United States Air Force, damage repair strategies are of great importance. Repair methods used in composite structures differ significantly from those used for metallic structures. Whereas metallic structures are typically repaired by bolted, riveted, or bonded patches, composite structures are commonly repaired by scarfing out the damaged area and filling the scarfed area with layers of composite material that produce the same stiffness as the material removed. One advantage of scarf repairs is their efficiency in restoring load carrying capacity to a composite laminate or structure. A through-thickness scarf joint is capable of restoring joint strengths close to that of the original composite laminate [1]. Another important advantage is that the repaired surface can retain the surface profile of the original structure, which is important in maintaining performance characteristics. However, scarf repairs require the removal of a significant amount of undamaged material to achieve the optimum scarf bond angle and restore strength. Thus, one of the primary design variables in the repair is the scarf angle used. Previous studies of composite scarf joints have shown that the smaller the scarf angle used, the higher the resulting strength [1-3]. However, an important aspect of composite scarf repair is the ability to understand damage progressions and failure modes to instil confidence that the repaired structure will function as intended. Traditional assessment of scarf repair performance has focused on strength-based failure predictions using conventional finite element-based analysis. However, scarf repair failure is a complex, progressive fracture process, which cannot be accurately simulated with continuum approaches. Thus, for accurate demonstration of composite scarf repair performance, damage progressions leading to failure must be properly predicted and modeled in numerical simulations. To date, however, limited research has been performed supporting the development and validation of progressive damage modeling methods associated with composite scarf repairs. This paper describes an ongoing research program between the U.S. Air Force Research Laboratory (AFRL) and the University of Utah's Utah Composites Laboratory (UCL).

In this research investigation, composite scarf repairs are used as a platform for the further evaluation, development, and validation of the AFRL in-house research code BSAM, which implements the AFRL Discrete Damage Methodology (DDM) framework. To date, BSAM has been used for the simulation of damage in a variety of idealized composite geometries and damage states. This study aims to extend the use of BSAM beyond its research realm, and apply it to sustainment engineering problems supporting the United States Air Force's mission. A combined computational and experimental investigation is proposed to extend the use of BSAM to the simulation of damage progression and failure analysis of scarfed composite repairs through integration into a methodology that can be implemented within the United States Air Force. Such repairs produce added complexity to progressive damage modeling due to damage produced at the angled scarf joint interface between the parent material and the inserted repair material. A building-block approach is proposed that features a progression of simulations and experimental validations with increasing complexity while representing the characteristic features of the repair methodologies currently used to sustain airframes.

This study will employ a building-block approach as depicted in Figure 1-1. This approach will be applied to both experimental characterization and model performance assessments. Experimental characterization and model assessments will be investigated across multiple length scales, from coupon-level material characterization tests (bottom of the building block) to component-scale multi-axial structural tests (top of the building block). All experimental work will be performed on the well-established composite system, Hexcel IM7/8552 carbon/epoxy unitape prepreg with adhesive bonds implemented using 3M® AF-163 film adhesive. All composite panels and specimens will be fabricated at the UCL using autoclave and hot-press curing techniques.

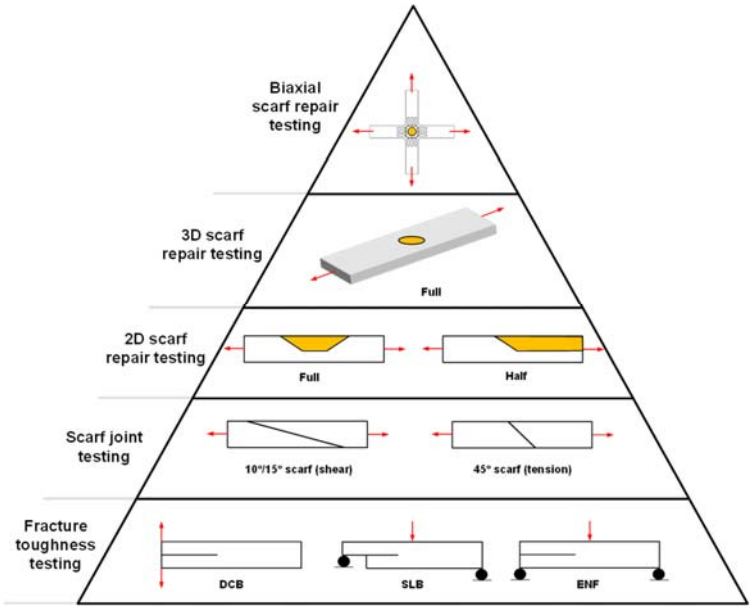

Figure 1-1: Experimental and numerical scarf-repair building block.

1.1 Material Characterization and Model Calibration

Stiffness, strength and fracture properties of the Hexcel IM7/8552 carbon/epoxy composite system are readily available in the open literature, and from previous material characterization at the UCL. In this study, material characterization will focus primarily on characterization of the fracture properties associated with the bondline between the parent composite material and the scarf repair material, both of which will be IM7/8552 carbon/epoxy. To this end, mode-I, mode-II, and mixed-mode I-II tests will be performed using the double cantilever beam (DCB), end-notch-flexure (ENF), and single-leg-bend (SLB) tests, respectively. The SLB test was selected over the mixed-mode-bend (MMB) test, due to its simplicity. The SLB test provides a mixed-mode I/II ratio of 0.4, and utilizes the same 3-point bend fixture as the ENF test. Although all three tests are well established for characterization of brittle fracture in composites, the existing LEFM-based methods of data reduction for these tests are not appropriate for highly-nonlinear film adhesives. Instead, this study will adopt a newly developed method for extraction of nonlinear fracture parameters using the J-integral approach [4-6]. This approach relies on digital image correlation (DIC) to capture the nonlinear deformation of the adhesive during the fracture process, and can be used to directly extract the traction-separation behaviour (a.k.a. the cohesive law) during mode I, mode II, or mixed-mode I/II loading.

To gain further confidence into BSAM's mixed-mode cohesive-law input parameters, a series of calibration tests will be performed on simple, through-thickness 2D scarf joint configurations as shown in Figure 1-2. Through-thickness 2D scarf joints will be designed to exhibit failure that transitions from shear-dominated (low scarf angle) to tension-dominated (high scarf angle). Based on previous experience, scarf angles of 5° will consist of shear-dominated failures, 45° will display tension-dominated failures, and 10° will consist of mixed-mode failures. Because these tests are inherently unstable (i.e. there is very little progression of damage prior to ultimate failure), global force-displacement data will be used for model validation. Additionally, a simplified configuration using metallic adherends will be examined first in an effort to test BSAM's nonlinear adhesive property capabilities without the complication of adherend matrix cracking.

Figure 1-2: Schematic of a simple, 2D through-thickness scarf joint.

1.2 2D & 3D Scarf Repairs in Tension and Flexure

For initial assessment and validation of the BSAM approach for analyzing composite scarf repairs, testing and analysis of idealized two-dimensional scarf repair specimens will be employed. The idealized 2D scarf repair specimen will be designed to incorporate representative scarf repair geometries and to produce different damage progressions and failure mechanisms. As illustrated in Figure 1-3, the "half-scarf" specimens will contain a 2D cross-section of the scarf joint repair, representative of the full-scale 3D scarf repair envisioned for use on composites aircraft structures. Initial sets of specimens will be designed for uniaxial tension and four-point flexure loading. Specimens will feature the scarf repair interface in the central region, and regions of both scarfed parent material and added repair material at one end as shown in Figure 3. Additional 2D idealized scarf repair specimens with a full length, two-sided scarf repair region will be fabricated and tested in tension and flexure (see level 3 of the building-block shown in Figure 1-1). During mechanical testing, DIC on the specimen cross-sectional surface will be used to provide direct comparison to displacement and strain fields obtained from BSAM. In addition, in situ ultrasonic inspection and acoustic emission will be performed to investigate the evolution of bondline decohesion, delaminations, and intralaminar cracking in the idealized 2D scarf repairs.

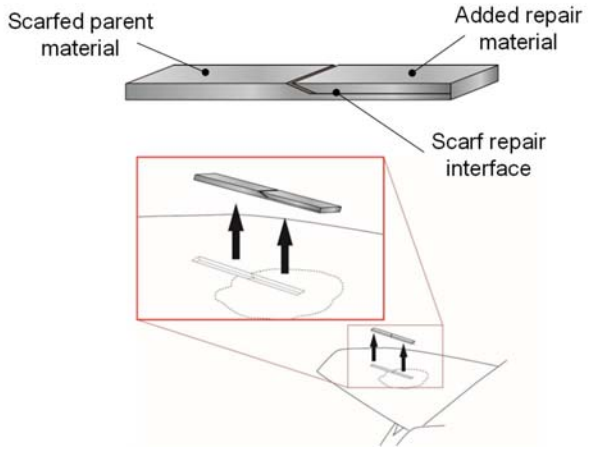

Figure 1-3: Schematic of an idealized half-scarf repair specimen configuration.

Following testing and BSAM analysis of the 2D idealized scarf repairs, full 3D plug-type scarf repairs (level 4 of the building-block shown in Figure 1-1) will be integrated into composite specimens for testing under tension and four-point flexure loading. The choice of scarf repair geometries and the required specimen dimensions will be determined based on results obtained from the 2D idealized scarf repair investigation as well as current best-practices for composite repair in the aircraft industry. DIC will be used on both the specimen edges and surfaces during testing to record strain variations during loading. Additionally, acoustic emission monitoring will be performed during loading to assist in identifying the occurrence of damage. Based on these indications, additional

interrupted tests may be performed, in which loading is halted and specimens are removed and subjected to X-ray computed tomography scanning and possibly destructive evaluation (e.g. sectioning, microscopy) to provide further information on damage progressions for subsequent validation of the BSAM modeling method.

1.3 Scarf Repairs under Biaxial Loading

The final step of the proposed building block will be a component-scale test of a full 3D scarf repair subjected to in-plane biaxial, tension-tension loading. To this end, a biaxial cruciform sample will be designed adopting a methodology presented in [7]. The overall dimensions of the cruciform sample will be sized in accordance with the required size of a realistic scarf repair. The planar dimensions, depth, and scarf angle of the repair will be selected based on consultation with technical experts in the USAF. The overall cruciform dimensions and stacking sequence will be optimized using linear (ABAQUS) and progressive-damage (BSAM) simulations, considering also the limitations of available planar biaxial test machines. The optimization process will be used to size the gage region and the loading arms to ensure that progressive damage of the scarf repair is not affected by the free edge effects or load introduction. A global system will be used to extract displacements and strains at the specimen boundaries (i.e. in cruciform arms), while a local, higher resolution system will be used to view strains in the gage region. In addition, an acoustic emission system will be used to determine initiation of damage within the scarf repair. Based on the acoustic emission data, the biaxial loading will be halted, the sample removed from the grips, and ultrasonically inspected. The combination of global load-displacement data, full-field strains, acoustic emission data, and ultrasonic C-scans will provide a clear picture of damage evolution necessary for validation of the BSAM progressive damage model described in the following section and how it can then be incorporated into an overall repair evaluation method.

2.0 DISCRETE DAMAGE MODELING METHODOLOGY

The DDM approach employed by BSAM represents networks of multiple parallel transverse matrix cracks within individual plies of a laminate and delamination between plies by coupling a Mesh Independent Crack (MIC) modeling technique [8-11] for arbitrary transverse matrix cracks and a cohesive zone model (CZM) [12] for the delamination between plies. This, combined with fiber failure [13-15] methods and nonlinear adhesive representations [16] completes the suite of damage modes expected in composite repair problems. As a detailed discussion of the mathematics behind these methods is beyond the scope of this paper, each of these damage modeling aspects will only be briefly described in the subsequent sections.

2.1 Regularized eXtended Finite Element for Matrix Cracking

Matrix cracks are modeled by using a regularized eXtented Finite Element Method (X-FEM). The regularized formulation (Rx-FEM) deals with continuous enrichment functions, and replaces the Heaviside step function typical of traditional X-FEM [17] with a continuous function changing from 0 to 1 over a narrow volume of the so called gradient zone. The formalism tying the volume integrals in the gradient zone to surface integrals in the limit of mesh refinement was discussed in [8,9]. The simulation begins without any initial matrix cracks, which then are inserted based on a failure criterion during the simulation. The LaRC04 [18] failure criterion is chosen in the present work. What is inserted is a CZM plane associated with a matrix crack, which then begins to open. The opening of the CZM, is performed by using the formulation [12] described briefly in section 2.2. Note that the delamination between the plies is also simulated by CZM, however, the cohesive elements between the interfaces are inserted during initial model preparation rather than resulting from a failure criteria.

2.2 Cohesive Zone Formulation for Crack and Delamination Propagation

A crack is inserted using the displacement enrichment necessary to model a displacement jump. The magnitude of the jump is initially zero and is controlled by an interface cohesive law [12]. The same cohesive law is used at the ply interfaces to represent potential delamination surfaces. The cohesive law used within BSAM is represented by a traction-separation curve consisting of two linear lines. Initially a steep positive portion of the curve is used to describe the elastic behavior across the displacement jump as if the jump did not exist. Once the traction level exceeds a specified cohesive strength (e.g. transverse tensile strength), the traction-separation law defines the reduction in traction in relation to the displacement jump, schematically shown in Figure 2-1a for a single loading mode (e.g. tension). Reference [12] describes the methodology for handling mixed-mode loading at a matrix crack or delamination crack tip, schematically shown in Figure 2-1b. A damage variable, d, is typically defined and tracked during the simulation. When d=1, the crack or delamination is fully damaged. The area under the traction-separation law is the critical value of energy release (G_{Ic}, G_{IIc}, or a mixed-mode value).

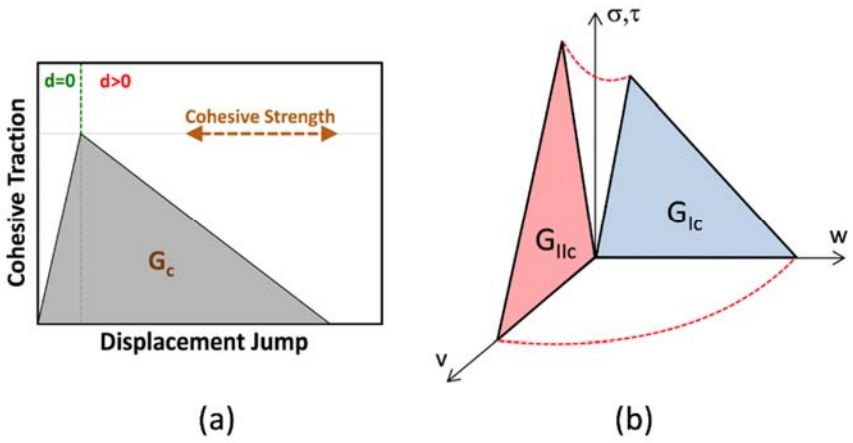

Figure 2-1: Schematic of typical traction-separation laws (a) single mode, (b) mixed-mode.

2.3 Fiber Fracture

In BSAM, fiber failure is handled by using two techniques. A statistical failure criteria called Critical Failure Volume (CFV) method [13] is used in problems where fiber failure has catastrophic character, e.g. open hole tension problems. The CFV approach adds effectively no burden associated with the fiber failure mode and therefore is more efficient and preferable where applicable. When the CFV criterion is satisfied, the simulation stops. The second approach represents Progressive Fiber Failure (PFF) methodology and is used in problems where fiber failure progression is important, e.g. saw cut composite panel problems and/or overheight compact tension (OCT) specimens [10]. This method is based on uniform degradation of the element stiffness when the fiber failure mode is detected [14,15]. At the time of writing, it is not clear which type of fiber failure modeling method, if any, will be most appropriate for use in composite scarf-repair problems.

2.4 Nonlinear Material Property Modeling

In BSAM, adhesive nonlinear response is represented via two methods. The first method is described in [16] and varies the shear modulus, G, as the minimum of a function of G with dilatational strain invariant (I_1) or a function of G with the distortional strain invariant (I_2). These G versus invariant curves are based on typical experimental adhesive testing. This method, while suitable for the problem described in [16], proved unstable in the current

effort. A second method was developed that varies Young's Modulus, E, or Poisson's ratio, ν, with I_1 and G with I_2. In practice, the second method has proven more effective and generally has been implemented by holding ν constant, varying G, and having BSAM calculate the appropriate E as will be described subsequently.

3.0 SELECTED RESULTS TO-DATE

The research effort described in this paper is relatively new and many tasks have not yet been addressed at the time of writing. However, significant progress has been made in the early objectives, some of which will be described here.

3.1 J-Integral Extraction of Fracture Parameters from DCB and ENF Testing

As described in Sec. 1.1, a new J-integral approach was adopted for extraction of the mode I and mode II cohesive laws for the AF-163 film adhesive. To gain confidence in this relatively new experimental method, several IM7/8552 DCB and ENF composite samples were tested without the film adhesive, and the resulting values of G_{Ic} and G_{IIc} were compared to those obtained from more traditional LEFM-based approaches. After validation of the J-integral approach, this method was applied to DCB and ENF samples with IM7/8552 adherents bonded with a single layer of the AF-163 film adhesive placed in the midplane.

3.1.1 Co-Cured IM7/8552 Specimens

The IM7/8552 DCB and ENF specimens were manufactured and tested according to ASTM guidelines for Mode I and Mode II interlaminar fracture toughness testing. As suggested by each ASTM standard (DCB: D5528, ENF: D7905), only one side of each sample was needed to observe delamination growth. The other side painted with a DIC speckle pattern around the crack-tip, and used to extract the required displacement fields needed for the J-integral approach [4-6]. Examples of the DIC-derived cohesive laws from DCB and ENF tests are shown in Figure 3-1a and 3-1b, respectively. Fracture toughness for each loading mode were

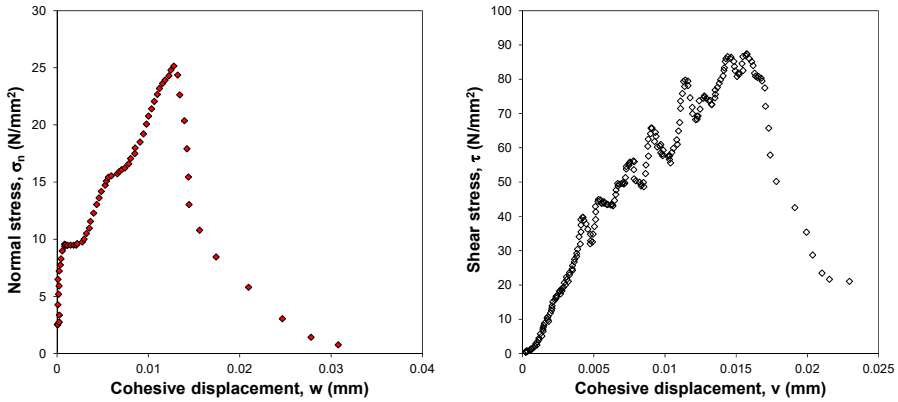

a) DCB (mode-I) b) ENF (mode-II)

Figure 3-1: Experimentally derived cohesive laws for unidirectional IM7/8552 carbon/epoxy composite extracted using digital image correlation.

calculated using the area under the corresponding traction-separation curves, yielding values of G_{Ic} = 0.26 N/mm and G_{IIc} = 0.97 N/mm. The ASTM standard methodology yielded values of G_{Ic} = 0.29 N/mm and G_{IIc} = 1.31 N/mm, indicating reasonable consistency with the J-integral approach. The small differences between the two methods were likely related to inaccuracies in extraction of the cohesive displacements using DIC, and variability in elastic material properties needed for calculation of the mode I and mode II J-integrals.

3.1.2 Adhesive Bonded Specimens

After validation described above, the J-integral method was used on DCB and ENF specimens bonded in the midplane with AF-163 film adhesive. Five DCB and ENF specimens were tested, and the respective force-displacement data are show in Figures 3-2a and 3-2b. As seen in Fig. 3-2a, the mode-I fracture of AF-163 adhesive was relatively linear, and similar in behaviour to what is typically observed in brittle materials. Conversely, the mode-II fracture shown in Fig. 3-2b exhibited highly nonlinear deformation and stable fracture propagation (note: brittle fracture in ENF tests is typically unstable). The J-integral approach was used to extract the cohesive behaviour from each sample, and the resulting traction-separation curves for mode I and mode II fracture are shown in 3-3a and 3-3b, respectively. As seen in Fig. 3-3a, the mode I traction-separation curves are nearly triangular, which is indicative of brittle fracture. Conversely, the mode II traction-separations curves can be described as trapezoidal, indicating large crack tip plasticity prior to adhesive decohesion. Note that these traction-separation laws are not unique to AF-163 film adhesive, and have been previously observed in other similar materials (e.g. FM-300 studied in Ref. [4] and [6]). The traction-separation curves shown in Fig. 3-3a and 3-3b were used to obtain three cohesive-zone parameters (i.e. fracture toughness, cohesive strength, and penalty stiffness) for each mode of fracture. These parameters, which are presented in Tables I and II, shown good correlation with the available values published by 3M®

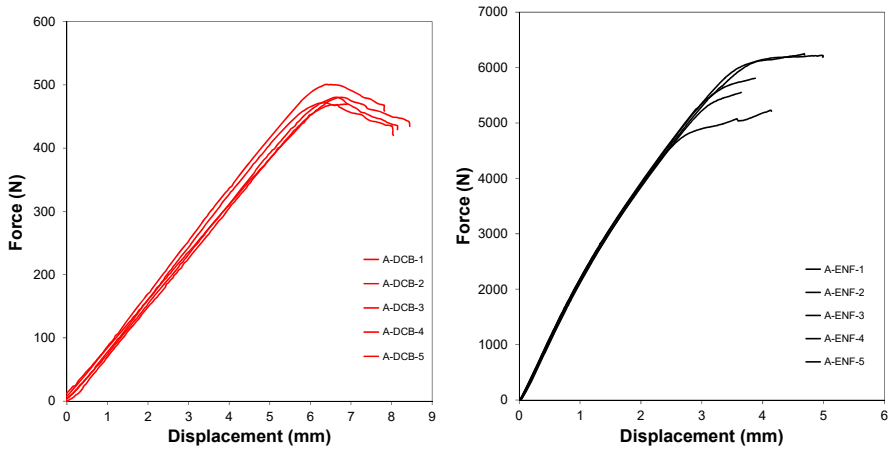

a) DCB (mode-I) b) ENF (mode-II)

Figure 3-2: Force-displacement curves from DCB and ENF adhesive fracture tests.

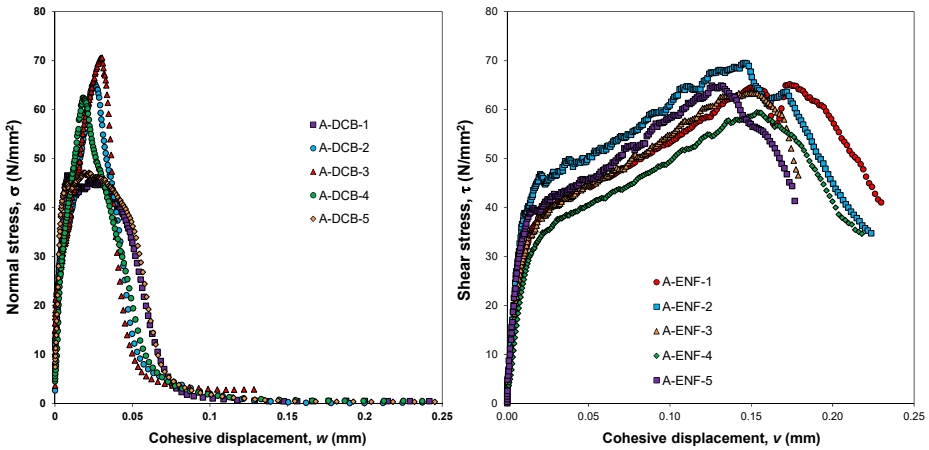

a) DCB (mode-I) b) ENF (mode-II)

Figure 3-3: Experimentally derived cohesive laws for AF-163 adhesive extracted using digital image correlation.

Table I. Cohesive model parameters from DCB adhesive tests

Specimen	G_{Ic} (N/mm)	σ_{max} (N/mm^2)	K_n (N/mm^3)
AVERAGE	**2.45**	**58.39**	**4161.15**
STD DEV (%)	4.80	18.76	78.39
Published	**2.63-4.38**	**48.20**	-

Table II. Cohesive model parameters from ENF adhesive tests

Specimen	G_{IIc} (N/mm)	τ_{max} (N/mm^2)	K_s (N/mm^3)
AVERAGE	**10.16**	**64.48**	**2681.34**
STD DEV (%)	13.27	5.62	26.36
Published	-	**47.90**	-

3.2 Nonlinear Material with Cohesive Zone Disbonding

As described in Section 2.2, the cohesive law implemented within BSAM is represented by a traditional traction-separation curve consisting of two straight lines. This formulation presents a challenge when trying to represent the observed behaviour of AF-163 adhesive, particularly during shear-dominated loading scenarios. To circumvent this issue, the fracture behaviour of AF-163 adhesive was approximated herein by combining the linear cohesive-zone model (Sec. 2.2) with the nonlinear material model (Sec. 2.4). This was achieved by placing a standard cohesive element in series with a nonlinear continuum element, as shown in Fig. 3-4a.

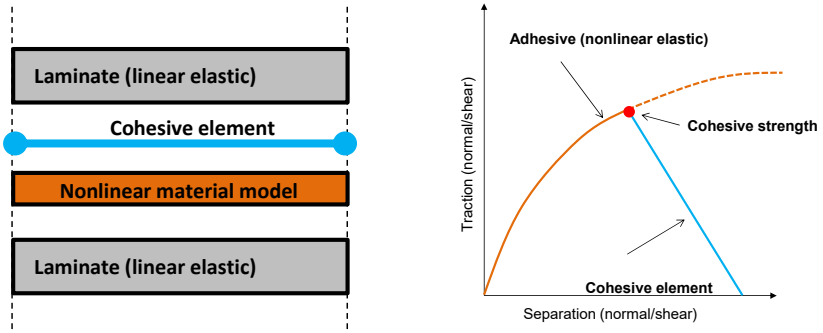

a) Non-standard cohesive zone model b) Resulting behavior

Figure 3-4: Definition of a new "non-standard" cohesive zone behaviour for AF-163 film adhesive.

As shown in Fig. 3-4b, placement of the two elements in series assures that: a) the initial portion of the new "non-standard" cohesive law is controlled by the nonlinear material model, and b) the unloading portion is controlled by the cohesive law. The nonlinear part of the traction-separation curve (orange) can be obtained directly from the experimental data shown in Figs. 3-3a-b prior to reaching the peak stress. The unloading part of the traction-separation curve (blue) initiates when the stress in both elements reaches the appropriate cohesive strength. The rate of unloading (i.e. slope of the blue curve) is controlled by appropriate selection of re-calibrated mode I and mode II fracture toughness parameters.

3.2.1 Initial Calibration Methodology and Results

Implementation and initial calibration of the non-standard cohesive law described above was performed using a simple patch test. The patch test consisted of two elastic elements representing the adherents (i.e. composite laminate), an element with the nonlinear behaviour representing the adhesive, and a zero-thickness cohesive zone element. Results of the patch test for both mode I and mode II loading are presented in Figure 3-5a-b. As seen in this figure, the proposed non-standard cohesive law accurately captures the initial nonlinearity, peak stress, and softening for each mode of loading.

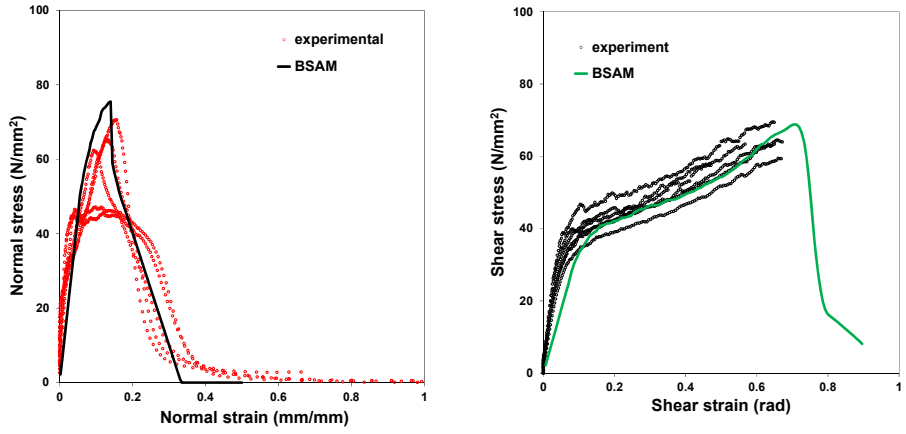

a) Mode-I cohesive behavior b) Mode-II cohesive behavior

Figure 3-5: Stress-stress behaviour of patch elements with the non-standard cohesive law.

After initial calibration using the patch tests, the nonstandard cohesive law was used to simulate the force-displacement response of the DCB, ENF, and SLB specimens bonded with the AF-163 film adhesive. Note that the SLB data were not used in the initial calibration, but instead, were used to determine if the proposed approach can accurately approximate the mixed-mode loading conditions. This check was necessary because of the non-similarity in shape of the traction-separation curves obtained for the AF-163 adhesive. As shown in Figure 3-6a, for brittle materials shape of the traction-separation law, regardless of mode mixity, can be approximated as triangular. As a result, interpolation of the mixed-mode I-II parameters is rather straightforward. For film adhesives, the cohesive law changes shape depending on the mode mixity (see Figure 3-6b), and therefore requires additional attention.

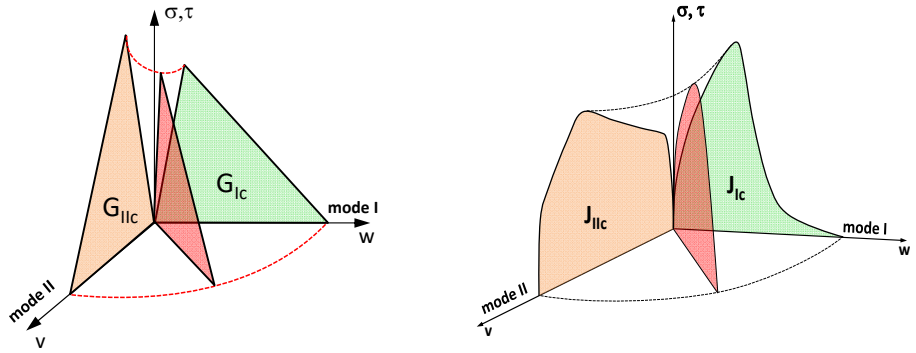

a) Standard mixed-mode cohesive law b) Non-standard mixed-mode cohesive law

Figure 3-6: Difference between standard (brittle) and non-standard (nonlinear) cohesive laws.

Results from simulating the DCB, ENF, and SLB tests using the non-standard cohesive law are presented in Fig. 3-7. In this figure, the colored symbols represent BSAM results, while the grey lines correspond to the experimental data. As seen in this figure, all three models accurately capture the nonlinearity in the initial loading, and correctly predict the force levels corresponding to the onset of adhesive decohesion. The force-displacement response after initiation of decohesion differed from the experimental data; however, the extent of decohesion for a given force-displacement level was nearly identical.

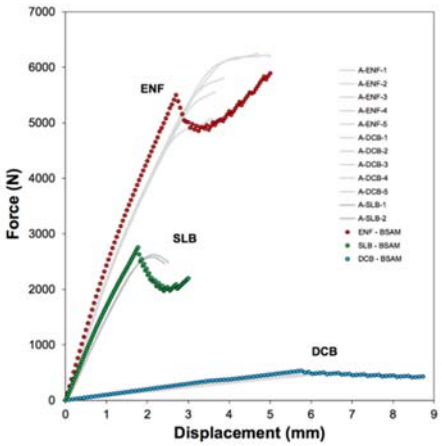

Figure 3-7: Simulated force-displacement data based on the proposed non-standard cohesive law.

4.0 CONCLUDING REMARKS

This work presents development of a combined experimental and numerical framework for simulation of damage evolution in composite scarf repairs. The initial efforts presented herein are focused on development of a methodology for simulation of nonlinear decohesion of film adhesives used in composite scarf repairs. To this end, an experimental J-integral approach was implemented for characterization of the nonlinear mode I, mode II, and mixed-mode I-II cohesive behaviour of 3M's AF-163 film adhesive. The data obtained from these experiments were used to definite a new non-standard cohesive zone behaviour, which was subsequently implemented in AFRL's progressive damage simulation tool, BSAM. Preliminary simulations of fracture characterization specimens showed good agreement with the experimental data, providing initial validation of the proposed approach. A near term goal of this project is to perform further validation of the new cohesive law using 2D composite scarf joints with varying scarf angles.

5.0 REFERENCES

[1] Zimmerman, K.B. and Liu, D., "An experimental Investigation of Composite Repair," Experimental Mechanics, Vol. 29, No. 11, p.1473-1487, 1996.

[2] Wang, C.H. and Gunnion, A., "On the Design Methodology of Scarf Repairs to Composite Laminates," Composites Science and Technology, Vol. 68, No. 1, p.35-46, 2008.

[3] Hart-Smith, J.L., "Adhesive-bonded Scarf and Stepped-lap Lap Joints," NASA Contract Technical Report, NAS1-11234, 1974.

[4] Girolamo, D., Davila, C.G., Leone, F.A. and Lin, S.Y., "Adhesive Characterization and Progressive Damage Analysis of Bonded Composite Joints" in Proceedings of the 2014 Pegasus-AIAA Student Conference; 23-25 Apr. 2014, Prague, Czechoslovakia.

[5] Zhao, Y., Seah, L.K., and Chai, G.B., "Measurement of Interlaminar Fracture Properties of Composites using the J-integral Method," Journal of Reinforced Plastics and Composites, Vol. 35, No. 14, p.1143-1154, 2016.

[6] Sarrado, C., Turon, A., Costa, J., and Renart, J., "An Experimental Analysis of the Fracture Behavior of Composite Bonded Joints in Terms of Cohesive Laws," Composites Part A: Applied Science and Manufacturing, Vol. 90, p.234-242, 2016.

[7] French, J., Rapking, D., Mollenhauer, D., and Czabaj, M.W., "Development of a Novel In-plane Tension-Tension Biaxial Cruciform Specimen," in Proceedings of the ASC 31st Technical Conference and ASTM D30 Meeting, Williamsburg, VA, 2016.

[8] Iarve, E.V. and Mollenhauer, D., "Numerical Modeling of Failure in Advanced Composite Materials", 1st Edition, Chapter 9: Mesh-Independent Matrix Cracking and Delamination Modeling in Advanced Composite Materials. eds. P. Camanho and S. Hallett, 2015.

[9] Iarve, E.V., Gurvich, M.R., Mollenhauer, D.H., Rose, A.C., and Davila, C.G., "Mesh-independent Matrix Cracking and Delamination Modeling in Laminated Composites," Int. J. Numerical Methods in Engineering, Vol. 88, No. 8, p. 749-773, 2011.

[10] Mollenhauer, D., Ward, L., Iarve, E.V., Putthanarat, S., Hoos, K., Hallett, S., and Li, X., "Simulation of Discrete Damage in Composite Overheight Compact Tension Specimens," Composites Part A, Vol. 43, No. 10, p.1667-1679, 2012.

[11] Swindeman, M., Iarve, E.V., Brockman, R.A., Mollenhauer, D.H., and Hallett, S.R., "Strength Prediction in Open Hole Composite Laminates by Using Discrete Damage Modeling," AIAA Journal, Vol. 51, No. 4, p.936-945, 2012.

[12] Turon, A., Camanho, P.P., Costa, J., and Dávila, C.G., "A Damage Model for the Simulation of Delamination in Advanced Composites Under Variable-mode Loading," Mechanics of Materials, Vol. 38, p.1072-1089, 2006.

[13] Iarve, E.V., Mollenhauer, D.H., Whitney, T.J., and Kim, R., "Strength Prediction in Composites with Stress Concentrations: Classical Weibull and Critical Failure Volume Methods with Micromechanical Considerations," Journal of Material Science, Vol. 41, No. 20, p. 6610-6622, 2006.

[14] Maimí, P., Camanho, P.P., Mayugo, J.A., and Dávila, C.G., "A Continuum Damage Model for Composite Laminates: Part I - Constitutive Model," Mechanics of Materials, Vol. 39, No. 10, p. 897-908, 2007.

[15] Maimí, P., Camanho, P.P., Mayugo, J.A., and Dávila, C.G., "A Continuum Damage Model for Composite Laminates: Part II - Computational Implementation and Validation," Mechanics of Materials, Vol. 39, No. 10, p. 909-919, 2007.

[16] Breitzman, T., Iarve, E., Cook, B., Schoeppner, G., and Lipton, R., "Optimization of a Composite Scarf Repair Patch under Tensile Loading," Composites: Part A, Vol. 40, p. 1921-1930, 2009.

[17] Moes, N., Dolbow, J., Belytschko, T., "A Finite Element Method for Crack Growth without Remeshing," Int. J. Num. Meth. Eng., Vol.46, p. 601-620, 1999.

[18] Pinho, S.T., Dávila, C.G., Camanho, P.P., Iannucci, L., and Robinson, P., "Failure Models and Criteria for FRP under In-Plane or Three-Dimensional Stress States Including Shear Non-Linearity," Hampton, VA, NASA/TM-2005-213530, 2005.